



Article

# Analysis of Von Kármán Swirling Flows Due to a Porous Rotating Disk Electrode

James Visuvasam <sup>1</sup> and Hammad Alotaibi <sup>2,\*</sup>

<sup>1</sup> Department of Mathematics, Rathnavel Subramaniam College of Arts and Science (Autonomous), Coimbatore 641 402, Tamil Nadu, India

<sup>2</sup> Department of Mathematics and Statistics, Faculty of Science, Taif University, P.O. Box 11099, Taif 21944, Saudi Arabia

\* Correspondence: hm.alotaibi@tu.edu.sa

**Abstract:** The study of Von Kármán swirling flow is a subject of active interest due to its applications in a wide range of fields, including biofuel manufacturing, rotating heat exchangers, rotating disc reactors, liquid metal pumping engines, food processing, electric power generating systems, designs of multi-pore distributors, and many others. This paper focusses on investigating Von Kármán swirling flows of viscous incompressible fluid due to a rotating disk electrode. The model is based on a system of four coupled second-order non-linear differential equations. The purpose of the present communication is to derive analytical expressions of velocity components by solving the non-linear equations using the homotopy analysis method. Combined effects of the slip  $\lambda$  and porosity  $\gamma$  parameters are studied in detail. If either parameter is increased, all velocity components are reduced, as both have the same effect on the mean velocity profiles. The porosity parameter  $\gamma$  increases the moment coefficient at the disk surface, which monotonically decreases with the slip parameter  $\lambda$ . The analytical results are also compared with numerical solutions, which are in satisfactory agreement. Furthermore, the effects of porosity and slip parameters on velocity profiles are discussed.

**Keywords:** mathematical modeling; non-linear differential equations; rotating disk electrodes; homotopy analysis method



**Citation:** Visuvasam, J.; Alotaibi, H. Analysis of Von Kármán Swirling Flows Due to a Porous Rotating Disk Electrode. *Micromachines* **2023**, *14*, 582. <https://doi.org/10.3390/mi14030582>

Academic Editors: Yi Zhang and Limin Xiao

Received: 9 October 2022

Revised: 17 February 2023

Accepted: 18 February 2023

Published: 28 February 2023



**Copyright:** © 2023 by the authors. Licensee MDPI, Basel, Switzerland. This article is an open access article distributed under the terms and conditions of the Creative Commons Attribution (CC BY) license (<https://creativecommons.org/licenses/by/4.0/>).

## 1. Introduction

In fluid mechanics, swirling flows are a common phenomenon, which have attracted significant attention due to their numerous industrial, mechanical, and environmental applications, such as rotating types of machinery (rotary pumps, fans, turbine, etc.), boilers, chemical storage, cyclone separators, and nuclear reactors spinning discs [1]. Rotating disk electrodes (RDE), incredibly porous and rough ones, are commonly used to measure electrochemical reactions, such as oxygen reduction reactions, catalysis, [2] and electrode kinetics [3]. Miklavcic et al. [4] studied the effect of slip parameters on various normalized slip coefficient ranges, and Turkyilmazoglu et al. [5] examined a swirling flow caused by a rotating rough and porous disk in terms of heat and mass transfer.

A disk with an infinite rotation was first described by Von Kármán in 1921 [6]. Von Kármán [6] also examined the similarity changes between partial and ordinary differential equations. Furthermore, Von Kármán formulated steady and unsteady states for this equation. Asymptotic solutions for steady-state conditions have been reported by Cochran [7], and non-steady-state solutions have been reported by Benton [8]. Millsaps and Pohlhausen [9] described the constant-temperature warmness switch values from a rotating disk using various Prandtl numbers.

Attia et al. [10–12] described how an external uniform magnetic field affects the flow caused by a rotating disk. Stuart [13], Kuiken [14], and Ockendon [15] investigated steady hydrodynamic flow induced by a rotating disk with the effect of uniform injection or suction. Using homotopy analysis, Rashidi et al. [16] derived approximate analytical

solutions for heat transfer in porous mediums of steady flow over rotating disks. The numerical solution of a nonlinear partial differential equation in a rotating porous disk flow near rotating electrodes is achieved using finite difference techniques. It has been reported by Attia et al. [17] that heat transfer in a porous medium can be used to solve a range of differential equations applied to the steady flow over rotating disks.

In many problems of practical interest, many researchers have investigated the fluid flow over a rotating disk because it has various applications in a variety of engineering, industrial, and scientific fields. For example, Zhou et al. [18] presented a mathematical model for Maxwell nanofluid flow with heat transmission over a stretching porous rotating disk. Shafiq et al. [19] investigated the significance of non-linear thermal radiation on Darcy–Forchheimer Casson-water/glycerine nanofluid flow with a uniform magnetic field subject to a rotating disk. Moreover, recently, Alotaibi and Rafique [20] presented a comprehensive analysis of the micro-rotation effect on nanofluid flow generated by a vertical stretching Riga plate. Additional detailed discussions of some recent investigations in the field of nanofluids have been conducted by several researchers and can be found in many related works (see, for example, [21–26]).

No analytical solution has been found due to the non-linearities in the reduced differential equation. Mathematica, Maple, and MATLAB are generally employed to solve non-linear equations. Many researchers have adopted approximate analytic methods for non-linear problems. Homotopy perturbation methods (HPMs) [27], homotopy analysis methods (HAMs) [28], and variational iteration methods (VIMs) [29] are among them. Liao [30] describes an analytical technique (HAM) for solving non-linear problems without needing small/significant parameters. Homotopy [31] is a fundamental concept in topology that is the basis for this technique. A porous rotating disk electrode (PRDE) has recently been analyzed by Visuvasam et al. [32]. The mathematical solution will be analytical, whereas more often, this method will be numerical. The method can be applied to various systems and has been described in several publications [33–38]. This model can be better understood by reading [39–43] and their references.

To the best of our knowledge, no research has been conducted to investigate the general analytical expressions for the radial, tangential, and axial velocity components. Therefore, the principle aim of this work is to fill that gap by employing the homotopy analysis method, which has been successfully able to interpret the radial, tangential, and axial velocity components for all experimental values. It is expected that the findings of this study will not only be useful in providing excellent information regarding industrial and technical applications, but will also support previously published work.

## 2. Mathematical Formulation of the Problems

We consider an infinite porous rotating disk coinciding with the plane  $z = 0$  and with the space  $z > 0$  occupied by a viscous incompressible fluid. A steady motion is generated by the rotation of a disk at a constant rotation rate of  $\Omega$ , which is equivalent to a Darcy model [16,17]. The physical model is outlined in Figure 1. Assuming the flow is laminar, and using the system characteristics described in [33], the continuity and Navier–Stokes equations in cylindrical coordinates are expressed as follows:

$$\frac{u}{r} + \frac{\partial u}{\partial r} + \frac{\partial w}{\partial z} = 0 \tag{1}$$

$$\rho \left( u \frac{\partial u}{\partial r} - \frac{v^2}{r} + w \frac{\partial u}{\partial z} \right) + \frac{\partial p}{\partial r} = \mu \left( \frac{\partial^2 u}{\partial r^2} + \frac{1}{r} \frac{\partial u}{\partial r} - \frac{u}{r^2} + \frac{\partial^2 u}{\partial z^2} \right) - \frac{\mu}{K\varepsilon} u \tag{2}$$

$$\rho \left( u \frac{\partial v}{\partial r} - \frac{uv}{r} + w \frac{\partial v}{\partial z} \right) = \mu \left( \frac{\partial^2 v}{\partial r^2} + \frac{1}{r} \frac{\partial v}{\partial r} - \frac{v}{r^2} + \frac{\partial^2 v}{\partial z^2} \right) - \frac{\mu}{K\varepsilon} v \tag{3}$$

$$\rho \left( u \frac{\partial w}{\partial r} + w \frac{\partial w}{\partial z} \right) + \frac{\partial p}{\partial z} = \mu \left( \frac{\partial^2 w}{\partial r^2} + \frac{1}{r} \frac{\partial w}{\partial r} + \frac{\partial^2 w}{\partial z^2} \right) - \frac{\mu}{K\varepsilon} w \tag{4}$$

where  $u$ ,  $v$ , and  $w$  are the radial, the angular, and  $\gamma = \frac{v}{K\Omega\varepsilon}$  the axial velocity components, respectively. In Equations (1) and (2),  $r$  and  $z$  are the radial and axial coordinates, respectively,  $p$  is the pressure,  $\rho$  is the bulk of the fluid, and  $\nu$  is the kinematic viscosity of the fluid. The partial slip boundary conditions for Equations (1)–(4) are described as follows [44]:

$$u(z = 0) = \lambda_1 \bar{\tau}_{rz}(z = 0), \quad v(z = 0) = \lambda_2 \bar{\tau}_{\varphi z}(z = 0) \tag{5}$$

where  $\tau_{rz}$  and  $\tau_{\varphi z}$  are the wall shear stresses, and  $\lambda_1$  and  $\lambda_2$  are two coefficients. Introducing the following dimensionless [32] variables

$$\zeta = \frac{z}{\sqrt{\frac{\nu}{\Omega}}}, \quad F = \frac{u}{\Omega r}, \quad G = \frac{v}{\Omega r}, \quad H = \frac{w}{\sqrt{\Omega \nu}}, \quad P = \frac{p_\infty - p}{\rho \nu \Omega}, \quad \lambda = \lambda_1 \sqrt{\frac{\Omega}{\nu}} \mu \tag{6}$$

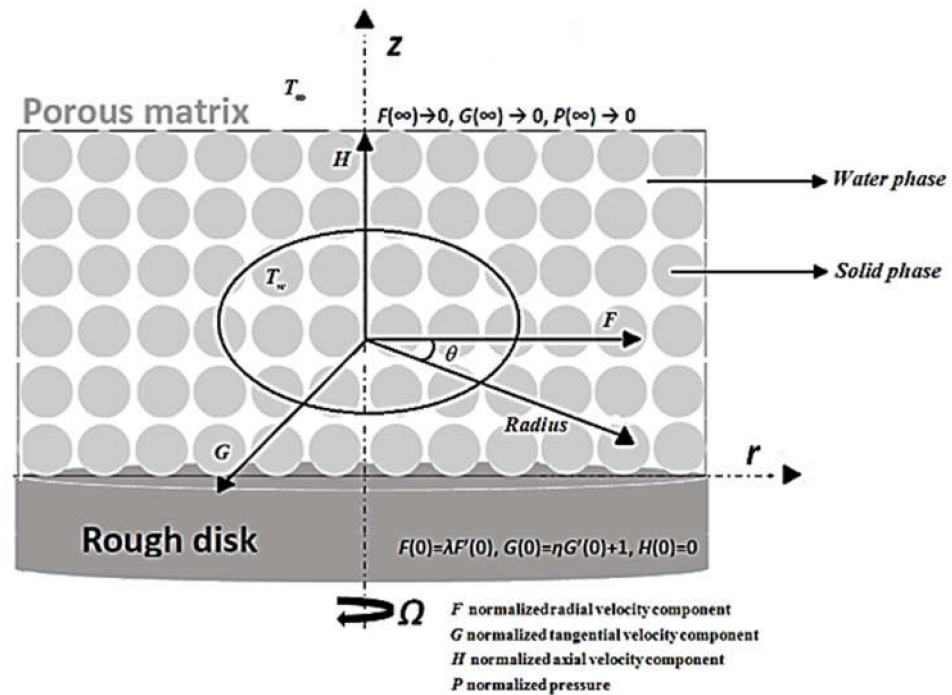


**Figure 1.** The coordinate system of the Von Kármán flow in a porous medium with its boundary conditions.

Equations (1)–(4) can be rewritten in following the dimensionless form [44]:

$$\frac{dH}{d\zeta} + 2F = 0 \tag{7}$$

$$\frac{d^2F}{d\zeta^2} - H \frac{dF}{d\zeta} - F^2 + G^2 - \gamma F = 0 \tag{8}$$

$$\frac{d^2G}{d\zeta^2} - H \frac{dG}{d\zeta} - 2FG - \gamma G = 0 \tag{9}$$

$$\frac{d^2H}{d\zeta^2} - H \frac{dH}{d\zeta} + \frac{dP}{d\zeta} - \gamma H = 0 \tag{10}$$

where  $F, G$  and  $H$  represent the velocity components and  $\gamma = \nu/K\Omega\varepsilon$  is the porosity parameter. The non-dimensional boundary conditions are obtained as follows:

$$F(\zeta = 0) = \lambda F'(\zeta = 0), G(\zeta = 0) = \eta G'(\zeta = 0) + 1, H(\zeta = 0) = 0 \tag{11}$$

$$\text{and } F(\zeta \rightarrow \infty) = 0, G(\zeta \rightarrow \infty) = 0, P(\zeta \rightarrow \infty) = 0 \tag{12}$$

### 3. Analytical Expressions of Velocity Components Using the Homotopy Analysis Method

In 1992, Liao [45–48] first reported HAM as a semi-exact methodology for solving non-linear equations. Some of the most characteristic examples of HAM are found in viscous flows of non-Newtonian fluids [49], KdV-type equations [50], finance [51], and non-linear optimal control problems [52], among others. Therefore, HAM is a useful methodology for solving non-linear problems analytically. In this model, the dimensionless concentrations of radial, tangential, and axial velocity components are approximated analytically using the HAM approach (see Appendix A for more information).

$$F(\zeta) = (A_2 + A_5)e^{-\sqrt{\gamma}\zeta} - \left( \frac{e^{-2\sqrt{\gamma}\zeta}}{3\gamma} \right) \left( A_1^2 + h \left( \frac{11}{6} A_3 A_1^2 \left( h + \frac{4}{11} \right) (\sqrt{\gamma})^3 + \frac{A_1^2}{60} \left( \frac{45}{2} A_2 \gamma e^{-\sqrt{\gamma}\zeta} - A_1^2 e^{-2\sqrt{\gamma}\zeta} \left( h + \frac{4}{3} \right) \right) \right) \right) \quad (13)$$

$$G(\zeta) = (A_1 + A_4)e^{-\sqrt{\gamma}\zeta} + \frac{1}{24} \frac{A_1 e^{-3\sqrt{\gamma}\zeta} h \left( -12\gamma^{5/2} \zeta e^{2\sqrt{\gamma}\zeta} + A_1^2 \sqrt{\gamma} - 6A_3 \gamma^2 e^{2\sqrt{\gamma}\zeta} \right)}{\gamma^{5/2}} \quad (14)$$

$$H(\zeta) = \frac{2h}{\sqrt{\gamma} e^{\sqrt{\gamma}\zeta}} \left( A_5 + \frac{A_2}{h} \right) + A_3 + A_6 - \frac{A_3 A_1^2 h^2}{\gamma^2 e^{2\sqrt{\gamma}\zeta}} \left( \frac{11}{18} + \frac{2}{9h} - \frac{1}{6\sqrt{\gamma}} - \frac{\zeta}{3} \right) - h \left( \frac{A_2 A_1^2}{12(\sqrt{\gamma})^5 e^{3\sqrt{\gamma}\zeta}} - \frac{2A_1 A_4 + A_2 - \frac{A_1^2}{h}}{3(\sqrt{\gamma})^3 e^{2\sqrt{\gamma}\zeta}} + \frac{A_3 A_2 (1 + \sqrt{\gamma}\zeta)}{2\gamma e^{\sqrt{\gamma}\zeta}} - \frac{A_1^4 (3h + 4)}{1080(\sqrt{\gamma})^7 e^{4\sqrt{\gamma}\zeta}} \right) \quad (15)$$

where  $A_i$ 's are constants which are given in Equations (A19), (A26), and (A27).

### 4. Numerical Simulations

The precision of the approximate solution obtained with HAM was calculated using symbolic software MATLAB [53] with code bvp4c. Based on a comparison, the analytical results obtained were compatible with the numerical results. Recently, Bikash Sahoo et al. [44] settled the non-linear differential equation system using multiple shooting methods. The homotopy analysis method was compared with the numerical method (MATLAB) and the simulation result provided by Bikash Sahoo et al. [44]. A satisfactory agreement was obtained between both methods, as shown in Figures 2–4.

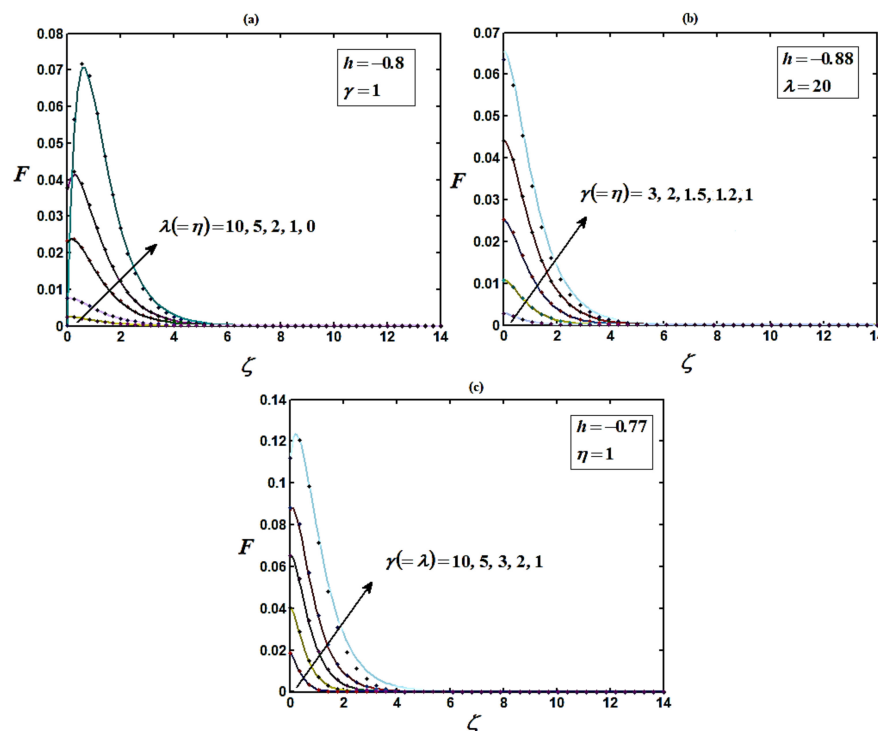


**Figure 2.** (a–c) Plots of the normalized radial velocity component  $F$  versus normalized distance from the disk  $\zeta$  using Equation (13) for various values of parameters. Solid lines represent Equation (13) and dotted lines represent the numerical solutions [44].

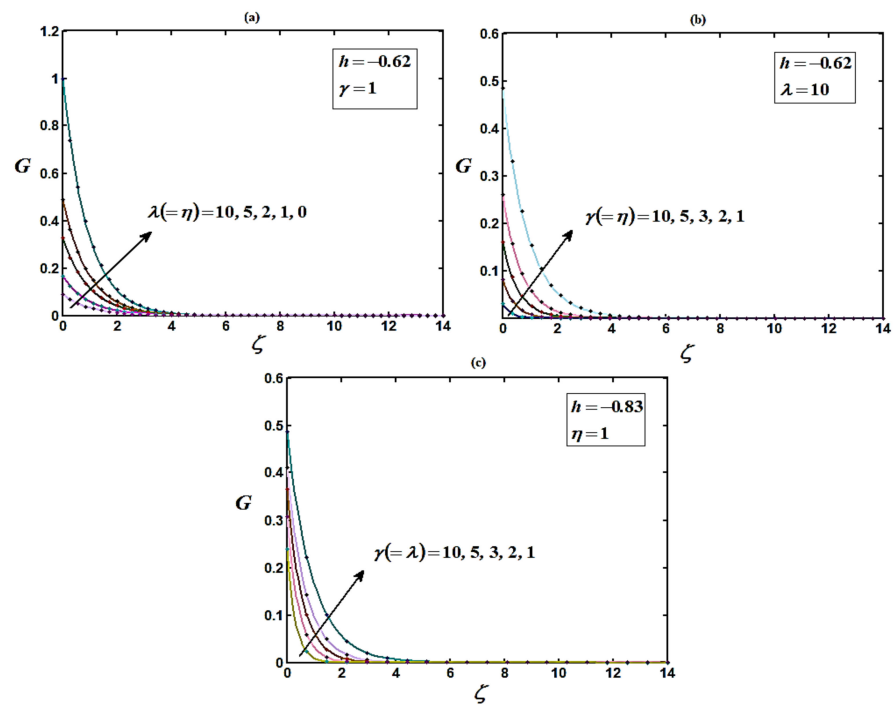


**Figure 3.** (a–c) Plots of the normalized tangential velocity component  $G$  versus normalized distance from the disk  $\zeta$  using Equation (14) for various values of parameters. Solid lines represent Equation (14) and dotted lines represent the numerical solutions [44].

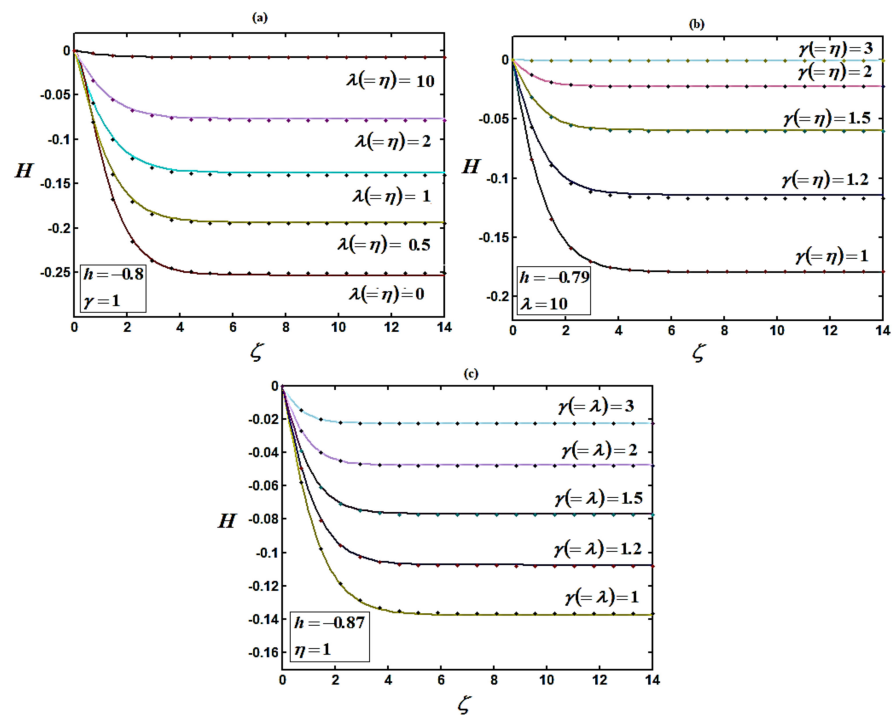


**Figure 4.** (a–c) Plots of the normalized axial velocity component  $H$  versus normalized distance from the disk  $\zeta$  using Equation (15) for various values of parameters. Solid lines represent Equation (15) and dotted lines represent the numerical solutions [44].

## 5. Discussion

Graphical representation of results is very useful to demonstrate the efficiency and accuracy of the homotopy analysis method for the above problem. This section describes the influence of some interesting parameters on the dimensionless radial, tangential, and axial velocity components. Equations (13)–(15) represent the general new analytical expressions for the dimensionless radial, tangential, and axial velocity components for  $\gamma \geq 1$  and for all values of other parameters. It is interesting to compare the impact of each constraint on the velocity components.

The boundary layer slip and porosity parameters are shown in Figures 2–4. Figure 2 illustrates that the radial velocity increases proportionally to  $\zeta$  increase. This pattern is followed until a maximum is reached its asymptotic value ( $G = 0$ ) at  $\zeta = 6$  and for all values of other parameters. The maximum amount of radial velocity decreases with increasing slip and porosity parameters, which causes the disk to move. Additionally, the radial velocity approaches its asymptotic values at the shortest distance from the disk for large amounts of parameters  $\lambda$ ,  $\mu$ , and  $\gamma$ .

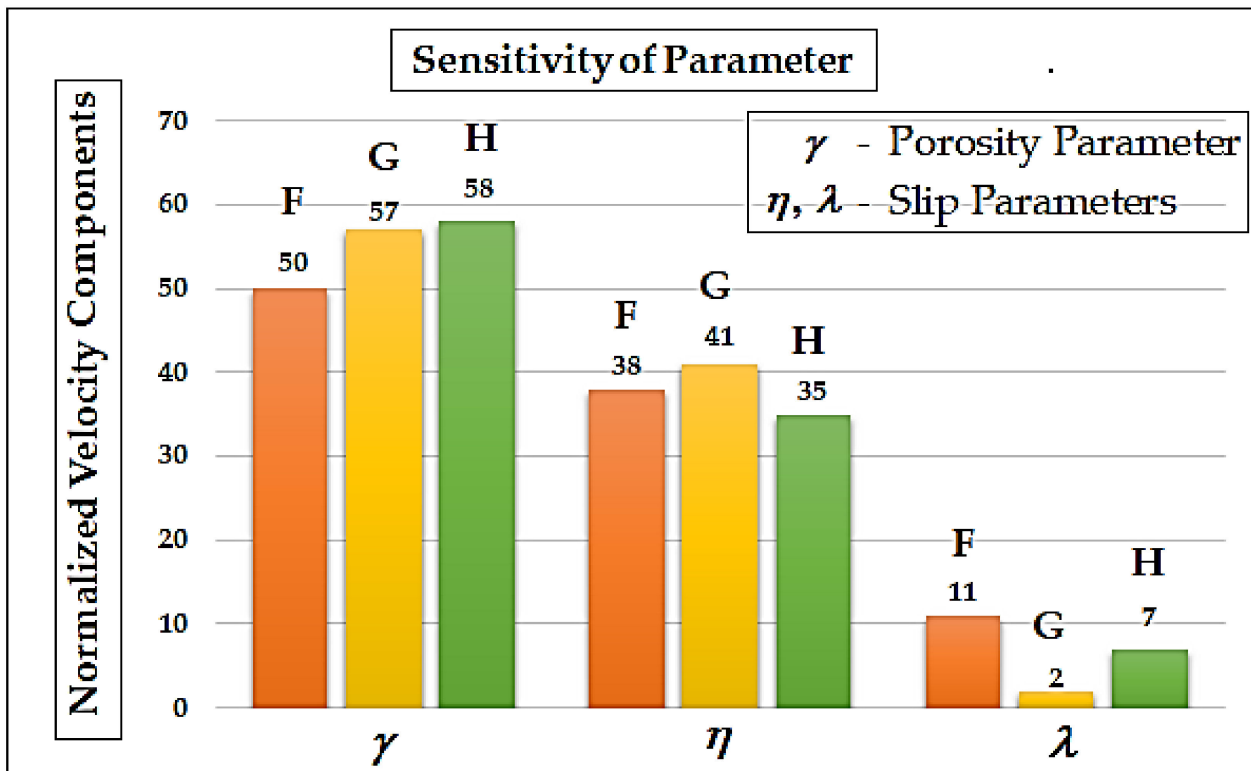
Figure 3 indicates the behavior of the tangential velocity for diverse values of the slip ( $\lambda$ ,  $\mu$ ) and porosity ( $\gamma$ ) parameters. The tangential velocity reaches its highest value at  $\zeta = 0$  and decreases monotonically to 0 as  $\zeta = 5$ . For the decreasing quantities of the slip and porosity parameters, axial pace movements in the direction of the disk for its minimum and magnitude also decrease.

Figure 4 indicates that for the increasing values of the slip  $\lambda$  and porosity  $\gamma$  parameters, the steady-state axial velocity increases. Additionally, decreases in porosity parameter leads to reductions in the vertical velocity components at infinity. This is due to the rigidity required by the fluid and the influence of the porosity of the medium. In Figure 4, it is also indicated that the axial velocity is maximum at  $\zeta = 0$ , then decreases slowly and remains constant at  $\zeta \geq 4$ . Figure 4 indicates that the vertical velocity component  $H$  reaches the full value at a finite distance ( $\zeta \geq 4$ ) from the disk. The gradual reduction of the peak in the radial component (Figure 1) with decreasing values porosity is reflected in the distributions of the axial velocity components (Figure 4a).

From Figures 2–4, it is observed that as the porosity increases the flow becomes more rigid, with the velocity components diminishing over most of the domain ( $0 \leq \gamma \leq 1$ ). The region close to the disk also contracts in size as porosity grows [44]. It is also observed that the reduction in the axial velocity  $H$  is higher than that in the radial velocity  $F$ , and much higher than that in the tangential velocity  $G$ . This is due to the entire effect of the centrifugal force, which is the source of radial and the vertical motion.

## 6. Differential Sensitivity Analysis of Parameters

Differential sensitivity analysis uses accumulated models that are partially differentiated. The partial derivative of slip parameters (dependent variables) has allowed us to find the partial derivative of porosity parameters (independent variables) at specific fixed experimental values of the parameters ( $\gamma = 1$ ,  $\lambda = \eta = 1$ , and  $\zeta = 1$ ). These parameters make it possible to determine the percentage of change in velocity components. Figure 5 shows the sensitivity analysis of the parameters. The porosity parameter  $\gamma$  has a greater impact on the variation of the velocity components than the slip parameter  $\eta$ , based on Figure 5. The remaining slip parameter  $\lambda$  accounts for only small changes in the velocity components. These results are also confirmed in Figure 5.



**Figure 5.** The sensitivity of parameters: percentage changes in normalized velocity components  $F$ ,  $G$  and  $H$  when  $\lambda = 1$ ,  $\eta = 1$ ,  $\gamma = 1$  at  $\zeta = 1$ .

## 7. Conclusions

An analysis of Von Kármán swirling flow and heat transfer in porous media has been presented in this paper. The coupled and highly nonlinear differential equations have been solved using the homotopy analysis method. Analysing the velocity component's behaviour using this analytical result will be valuable. Additionally, the effects and sensitivity analyses of porosity and slip parameters have been discussed. The semi-analytical expressions of the concentration were highly accurate compared to reliable numerical data. Furthermore, they had a greater influence on the heat transfer coefficient than the velocity slip parameter  $\lambda$ . The movement coefficient for maintaining the disk at a constant rotation rate was also enhanced by increasing values of  $\gamma$ . The method described here could easily be applied to the study of other Von Kármán swirling flows and heat transfers in porous media. In our study, we found that boundary layer thickness generally increased with time, but became constant once the steady state was reached; the radial and tangential flow velocities increased both over time and with separation from the disk surface, resulting in accelerated flows.

**Author Contributions:** Formulation done by J.V. and H.A.; Methodology, J.V.; Problem solved by J.V. and H.A.; All authors contributed equally to writing manuscript. All authors have read and agreed to the published version of the manuscript.

**Funding:** This research received no external funding.

**Data Availability Statement:** Not applicable.

**Acknowledgments:** The authors would like to acknowledge Deanship of Scientific Research, Taif University for funding this work.

**Conflicts of Interest:** The authors declare no conflict of interest.

**Abbreviations**

$C_m$	dimensionless moment coefficient (-);
$c_p$	heat capacity of the fluid at constant pressure (J/kg/K);
$F, G, H$	normalized radial, tangential, and axial velocity components (-);
$K$	Darcy permeability (m <sup>2</sup> );
$Nu$	Nusselt number (-);
$p, P$	pressure (Pa) and normalized pressure (-);
$Pr$	Prandtl number (-);
$q$	heat flux supplied to the disk (W/m <sup>2</sup> );
$r, \varphi, z$	cylindrical coordinates (m);
$Re$	rotational Reynolds number (-);
$T$	temperature (K);
$u, v, w$	radial, tangential, and axial velocity components (m/s);
$\beta$	normalized temperature slip factor (-);
$\beta_1$	proportionality constant (-);
$\varepsilon$	porosity (-);
$\gamma$	normalized porosity parameter (-);
$\kappa$	thermal conductivity of the fluid (W/(m K));
$\lambda, \eta$	normalized velocity slip parameters (-);
$\mu, \nu$	dynamic (Pa.s) and kinematic (m <sup>2</sup> /s) fluid viscosities;
$\Omega$	rotation rate of the disk (rad/s);
$\rho$	voluminal mass of the fluid (kg/m <sup>3</sup> );
$\zeta$	normalized distance from the disk (-);
$\theta$	normalized temperature (-);
$w$	denotes a quantity evaluated at the wall;
$\infty$	denotes a quantity evaluated at infinity;
'	denotes a derived quantity according to the axial direction.

**Appendix A**

*Analytical Solution of Equations (7)–(9) Using the Homotopy Analysis Method*

In this appendix, we derive the general new analytical solutions of non-linear Equations (7)–(9) using the homotopy analysis method. To find the solutions of Equations (7)–(9), we construct the homotopy as follows:

$$F'' - \gamma F + G^2 - ph(-HF' - F^2) = 0 \tag{A1}$$

$$G'' - \gamma G - ph(-HG' - 2FG) = 0 \tag{A2}$$

$$H' + 2F = 0 \tag{A3}$$

where  $p \in [0, 1]$  is the embedding parameter and  $h \neq 0$  is a non-zero auxiliary parameter.

The approximate solutions of Equations (7)–(9) are:

$$F = F_0 + F_1p + F_2p^2 + \dots \tag{A4}$$

$$G = G_0 + G_1p + G_2p^2 + \dots \tag{A5}$$

$$H = H_0 + H_1p + H_2p^2 + \dots \tag{A6}$$

Substituting Equations (A4)–(A6) in Equations (A1)–(A3) respectively results in:

$$(F_0 + F_1p + \dots) - \gamma(F_0 + F_1p + \dots) + (G_0 + G_1p + \dots)^2 + ph((H_0 + H_1p + \dots)(F_0 + F_1p + \dots) + (F_0 + F_1p + \dots)^2) = 0 \tag{A7}$$

$$(G_0 + G_1p + G_2p^2 + \dots) + \gamma(G_0 + G_1p + G_2p^2 + \dots) + ph\left(\begin{matrix} (H_0 + H_1p + H_2p^2 + \dots)(G_0 + G_1p + G_2p^2 + \dots) \\ + 2(F_0 + F_1p + F_2p^2 + \dots)(G_0 + G_1p + G_2p^2 + \dots) \end{matrix}\right) = 0 \tag{A8}$$

$$(H_0 + H_1p + H_2p^2 + \dots)' + 2(F_0 + F_1p + F_2p^2 + \dots) = 0 \tag{A9}$$

Comparing the coefficients of like powers of  $p$  in Equation (A7), we obtain:

$$p^0 : F_0'' - \gamma F_0 + G_0^2 = 0 \tag{A10}$$

$$p^1 : F_1'' - \gamma F_1 + 2G_0G_1 - h(-H_0F_0' - F_0^2) = 0 \tag{A11}$$

Comparing the coefficients of like powers of  $p$  in Equation (A8), we have:

$$p^0 : G_0'' - \gamma G_0 = 0 \tag{A12}$$

$$p^1 : G_1'' - \gamma G_1 - h(-H_0G_0' - 2F_0G_0) = 0 \tag{A13}$$

Analyzing the factors of similar powers of  $p$  in Equation (A9), we obtain:

$$p^0 : H_0' + 2(F_0) = 0 \tag{A14}$$

$$p^1 : H_1' + 2(F_1) = 0 \tag{A15}$$

The boundary conditions in Equations (12) and (13) become:

$$\begin{aligned} F_0(0) &= \lambda F_0'(0), G_0(0) = \eta G_0'(0) + 1, H_0(0) = 0 \\ F_i(0) &= \lambda F_i'(0), G_i(0) = \eta G_i'(0), H_i(0) = 0, F_{i-1}(\infty) = G_{i-1}(\infty) = 0 \forall i = 1, 2, 3 \dots \end{aligned} \tag{A16}$$

Solving Equations (A10) and (A4) and using the boundary conditions (A16), we find:

$$F_0(\zeta) = A_2 e^{-\sqrt{\gamma}\zeta} - \frac{1}{3} \frac{A_1^2 e^{-2\sqrt{\gamma}\zeta}}{\gamma} \tag{A17}$$

$$F_1(\zeta) = A_5 e^{-\sqrt{\gamma}\zeta} - \frac{e^{-4\sqrt{\gamma}\zeta} h}{3\gamma} \left( \begin{aligned} &\left( \frac{11}{6} A_3 A_1^2 \left( h + \frac{4}{11} \right) \gamma^{3/2} + \gamma^2 (A_1^2 A_3 h \zeta - 2 A_3 A_4 - A_2^2) \right) e^{2\sqrt{\gamma}\zeta} \\ &+ \frac{3}{4} A_2 A_3 (2\gamma^3 \zeta + \gamma^{5/2}) e^{3\sqrt{\gamma}\zeta} - \frac{1}{60} \left( -\frac{45}{2} A_2 \gamma e^{\sqrt{\gamma}\zeta} + A_1^2 \left( h + \frac{4}{3} \right) \right) A_1^2 \end{aligned} \right) \tag{A18}$$

where

$$\begin{aligned} A_1 &= \frac{1}{\sqrt{\gamma\eta+1}}, A_2 = \frac{A_1^2(2\sqrt{\gamma}\lambda+1)}{3\gamma(\sqrt{\gamma}\lambda+1)}, A_3 = \frac{A_1^2-6A_2\gamma}{3\sqrt{\gamma^3}}, \\ A_4 &= -\frac{1}{24} \frac{A_1 h (6A_3 \eta \gamma^4 + 3A_1^2 \eta \sqrt{\gamma} + A_1^2 - 6A_3 \sqrt{\gamma^3})}{\gamma^2 (\eta \sqrt{\gamma} + 1)} \end{aligned} \tag{A19}$$

Considering two iterations, we obtain

$$F(\zeta) \approx F_0(\zeta) + F_1(\zeta) \tag{A20}$$

After putting Equations (A17) and (A18) in (A20), the final results can be described as Equation (13) in the text. Similarly, solving Equations (A12) and (A13) and using the boundary conditions (A16), we obtain:

$$G_0(\zeta) = A_1 e^{-\sqrt{\gamma}\zeta} \tag{A21}$$

$$G_1(\zeta) = A_4 e^{-\sqrt{\gamma}\zeta} + \frac{1}{24} \frac{A_1 e^{-3\sqrt{\gamma}\zeta} h (-12\gamma^{5/2}\zeta e^{2\sqrt{\gamma}\zeta} + A_1^2 \sqrt{\gamma} - 6A_3 \gamma^2 e^{2\sqrt{\gamma}\zeta})}{\gamma^{5/2}} \tag{A22}$$

According to the HAM, we can obtain the solutions of Equation (9) as follows:

$$G(\zeta) \approx G_0(\zeta) + G_1(\zeta) \tag{A23}$$

After substituting Equations (A21) and (A22) in (A23), the final results can be described as Equation (14) in the text. Using the same procedure to solve Equations (A14) and (A15), we find:

$$H_0(\zeta) = \frac{2A_2 e^{-\sqrt{\gamma}\zeta}}{\sqrt{\gamma}} - \frac{A_1^2 e^{-2\sqrt{\gamma}\zeta}}{3\gamma^{3/2}} + A_3 \tag{A24}$$

$$\begin{aligned} H_1(\zeta) &= \frac{A_3 A_1^2 h^2}{\gamma^2 e^{2\sqrt{\gamma}\zeta}} \left( \frac{11}{18} + \frac{2}{9h} - \frac{1}{6\sqrt{\gamma}} - \frac{\zeta}{3} \right) + \frac{2A_5 h}{\sqrt{\gamma} e^{\sqrt{\gamma}\zeta}} \\ &- h \left( + \frac{A_2 A_1^2}{12(\sqrt{\gamma})^3 e^{3\sqrt{\gamma}\zeta}} - \frac{(2A_1 A_4 + A_2^2)}{3r^3 e^{2\sqrt{\gamma}\zeta}} + A_3 A_2 \left( \frac{1 + \sqrt{\gamma}\zeta}{2\gamma e^{\sqrt{\gamma}\zeta}} \right) - \frac{A_1^4 (3h+4)}{1080r^7 e^{4\sqrt{\gamma}\zeta}} \right) + A_6 \end{aligned} \tag{A25}$$

where

$$A_5 = \frac{h}{360(\lambda\sqrt{\gamma}+1)} \left( \begin{aligned} &\frac{320}{\gamma} \left( A_1^2 A_3 \lambda \left( h + \frac{1}{2} \right) - \frac{3}{4} A_1 A_4 - \frac{3}{8} A_2^2 \right) + 30\lambda (2A_1 A_4 + A_2^2 - \frac{3}{8\lambda} A_3 A_2) \\ &- \frac{8}{\gamma} \left( \left( \frac{1}{4} + \lambda \right) \left( h + \frac{4}{3} \right) \frac{A_1^4}{\gamma^2} - \frac{55}{2} \left( \frac{27}{44} A_2 \lambda + A_3 \left( h + \frac{4}{11} \right) \right) \frac{A_1^2}{\gamma} \right) + 45 \left( \frac{A_1^2}{(\sqrt{\gamma})^7} - 2A_3 \lambda \right) A_2 \end{aligned} \right) \tag{A26}$$

$$A_6 = \frac{h}{(\lambda\sqrt{\gamma}+1)} \left( \begin{aligned} &\left( A_1^2 A_3 \lambda \left( h + \frac{2}{3} \right) - \frac{2}{3} A_1 A_4 - \frac{1}{3} A_2^2 \right) \gamma + \left( \frac{A_1^2}{6r} - 2A_3 \lambda (\sqrt{\gamma})^3 \right) A_2 - \frac{A_1^4}{24} \left( h + \frac{4}{3} \right) \left( \frac{1}{5(\sqrt{\gamma})^3} + \frac{\lambda}{\gamma} \right) \\ &+ \frac{4A_1^2}{9} \left( \frac{3}{2} A_2 \lambda + A_3 \left( h + \frac{1}{2} \right) \right) - \lambda \left( 2A_1 A_4 + A_2^2 + \frac{A_3 A_2}{\lambda} \right) \gamma \end{aligned} \right) \tag{A27}$$

Additionally,

$$H(\zeta) \approx H_0(\zeta) + H_1(\zeta) \tag{A28}$$

Substituting Equations (A24) and (A25) in (A28), the final results can be described as Equation (15) in the text.

## References

1. Kataoka, H.; Tomiyama, A.; Hosokawa, S.; Sou, A.; Chaki, M. Two-phase swirling flow in a gas-liquid separator. *J. Power Energy Sys.* **2008**, *2*, 1120–1131. [[CrossRef](#)]
2. Bonnacaze, R.; Mano, N.; Nam, B.; Heller, A. On the behavior of the porous rotating disc electrode. *J. Electrochem. Soc.* **2007**, *154*, F44–F47. [[CrossRef](#)]
3. Vargas, R.; Borrás, C.; Mostanya, J.; Scharifker, B.R. Kinetics of surface reactions on rotating disk electrodes. *Electrochim. Acta* **2012**, *80*, 326–333. [[CrossRef](#)]
4. Miklavcic, M.M.; Wang, C.Y. The Flow due to a Rough Rotating Disk. *J. Appl. Math. Phys.* **2004**, *55*, 235–246. [[CrossRef](#)]
5. Turkyilmazoglu, M.; Senel, P. Heat and mass transfer of the flow due to a rotating rough and porous disk. *Int. J. Therm. Sci.* **2013**, *63*, 146–158. [[CrossRef](#)]
6. Kármán, T.V. Über laminare und turbulente Reibung. *ZAMM* **1921**, *1*, 233–252. [[CrossRef](#)]
7. Cochran, W.G. Flow due to a rotating disc. *Proc. Camb. Philos. Soc.* **1934**, *30*, 365–375. [[CrossRef](#)]
8. Benton, E.R. On the flow due to a rotating disk. *J. Fluid. Mech.* **1966**, *24*, 781–800. [[CrossRef](#)]
9. Millsaps, K.; Pohlhausen, K. Heat transfer by laminar flow from a rotating disk. *J. Aeronaut. Sci.* **1952**, *19*, 120–126. [[CrossRef](#)]
10. Attia, H.A. Unsteady MHD flow near a rotating porous disk with uniform suction or injection. *J. Fluid Dynam. Res.* **1998**, *23*, 283–290. [[CrossRef](#)]
11. Attia, H.A.; Aboul-Hassan, A.L. Effect of Hall Current on the Unsteady MHD Flow Due to a Rotating Disk with Uniform Suction or Injection. *Appl. Math. Model.* **2001**, *25*, 1089–1098. [[CrossRef](#)]
12. Attia, H.A. On the effectiveness of uniform suction-injection on the unsteady flow due to a rotating disk with heat transfer. *Int. Commun. Heat Mass* **2002**, *29*, 653–661. [[CrossRef](#)]
13. Stuart, J.T. On the effects of uniform suction on the steady flow due to a rotating disk. *Quart. J. Mech. Appl. Math.* **1954**, *7*, 446–457. [[CrossRef](#)]
14. Kuiken, H.K. The effect of normal blowing on the flow near a rotating disk of infinite extent. *J. Fluid Mech.* **1971**, *47*, 789–798. [[CrossRef](#)]
15. Ockendon, H. An asymptotic solution for steady flow above an infinite rotating disk with suction. *Quart. J. Mech. Appl. Math.* **1972**, *25*, 291–301. [[CrossRef](#)]
16. Rashidi, M.M.; Mohimaniyan Pour, S.A.; Hayat, T.; Obaidat, S. Analytic Approximate Solutions for Steady Flow over a Rotating Disk in Porous Medium with Heat Transfer by Homotopy Analysis Method. *Comput. Fluids* **2012**, *54*, 1–9. [[CrossRef](#)]
17. Attia, H. Steady flow over a rotating disk in porous medium with heat transfer. *Nonlinear Anal. Model. Cont.* **2009**, *14*, 21–26. [[CrossRef](#)]
18. Zhou, S.-S.; Bilal, M.; Khan, M.A.; Muhammad, T. Numerical Analysis of Thermal Radiative Maxwell Nanofluid Flow Over-Stretching Porous Rotating Disk. *Micromachines* **2021**, *12*, 540. [[CrossRef](#)]
19. Shafiq, A.; Rasool, G.; Alotaibi, H.; Aljohani, H.M.; Wakif, A.; Khan, I.; Akram, S. Thermally Enhanced Darcy-Forchheimer Casson-Water/Glycerine Rotating Nanofluid Flow with Uniform Magnetic Field. *Micromachines* **2021**, *12*, 605. [[CrossRef](#)]
20. Alotaibi, H.; Rafique, K. Numerical Analysis of Micro-Rotation Effect on Nanofluid Flow for Vertical Riga Plate. *Crystals* **2021**, *11*, 1315. [[CrossRef](#)]
21. Rasool, G.; Shafiq, A.; Alqarni, M.S.; Wakif, A.; Khan, I.; Bhutta, M.S. Numerical Scrutinization of Darcy-Forchheimer Relation in Convective Magnetohydrodynamic Nanofluid Flow Bounded by Nonlinear Stretching Surface in the Perspective of Heat and Mass Transfer. *Micromachines* **2021**, *12*, 374. [[CrossRef](#)] [[PubMed](#)]
22. Yan, Z.; Wang, J.; Wang, C.; Yu, R.; Shi, L.; Xiao, L. Optical microfibers integrated with evanescent field triggered self-growing polymer nanofilms. *Opt. Express* **2022**, *30*, 18044–18053. [[CrossRef](#)] [[PubMed](#)]
23. Zhang, Y.; Zhou, A.; Chen, S.; Lum, G.Z.; Zhang, X. A perspective on magnetic microfluidics: Towards an intelligent future. *Biomicrofluidics* **2022**, *16*, 011301. [[CrossRef](#)] [[PubMed](#)]
24. Shin, D.J.; Zhang, Y.; Wang, T.H. A droplet microfluidic approach to single-stream nucleic acid isolation and mutation detection. *Microfluid. Nanofluidics* **2014**, *17*, 425–430. [[CrossRef](#)]
25. Zhang, Y.; Wang, T.H. Micro magnetic gyromixer for speeding up reactions in droplets. *Microfluid. Nanofluidics* **2012**, *12*, 787–794. [[CrossRef](#)]
26. Lee, J.; Lee, S.; Lee, M.; Prakash, R.; Kim, H.; Cho, G.; Lee, J. Enhancing Mixing Performance in a Rotating Disk Mixing Chamber: A Quantitative Investigation of the Effect of Euler and Coriolis Forces. *Micromachines* **2022**, *13*, 1218. [[CrossRef](#)]
27. Dehghan, M.; Heris, J.M.; Saadatmandi, A. Application of semi-analytic methods for the Fitzhugh-Nagumo equation, which models the transmission of nerve impulses. *J. Math. Methods Appl. Sci.* **2010**, *33*, 1384–1398. [[CrossRef](#)]
28. Liao, S.J. *On the Analysis of Variable Thermophysical Properties of Thermophoretic Viscoelastic Fluid Flow Past a Vertical Surface with nth Order of Chemical Reaction. Beyond Perturbation, An Introduction to Homotopy Analysis Method*; Boca Raton Chapman Hall, CRC Press: Boca Raton, FL, USA, 2003.
29. Dehghan, M.; Salehi, R. Analytical Approach to Differential Equations with Piecewise Continuous Arguments via Modified Piecewise Variational Iteration Method. *Comput. Phys. Commun.* **2010**, *181*, 1255–1265. [[CrossRef](#)]
30. Wang, Z.K.; Cao, T.A. *An Introduction to Homotopy Methods*; Chongqing Publishing House: Chongqing, China, 1991.
31. Kamal, M.M.; Mohamad, A. Effect of Swirl on Performance of Foam Porous Medium Burners. *J. Combust. Sciand. Tech.* **2006**, *178*, 729–761. [[CrossRef](#)]

32. Visuvasam, J.; Molina, A.; Laborda, E.; Rajendran, L. Mathematical Models of the Infinite Porous Rotating Disk Electrode. *Int. J. Electrochem. Sci.* **2018**, *13*, 9999–10022. [[CrossRef](#)]
33. Muhammad, S.; Ghania, X.; Kottakkaran, S.N.; Muhammad, A.Z.R.; Muhammad, I.K.; Punith Gowda, R.J.; Prasannakumara, B.C. Ohmic heating effects and entropy generation for nanofluidic system of Ree-Eyring fluid: Intelligent computing paradigm. *Int. Commun. Heat Mass Transf.* **2021**, *129*, 105683.
34. Yun, -J.X.; Faisal, S.; Ijaz, K.M.; Naveen Kumar, R.; Punith Gowda, R.J.; Prasannakumara, B.C.; Malik, M.Y.; Sami, U.K. New modeling and analytical solution of fourth grade (non-Newtonian) fluid by a stretchable magnetized Riga device. *Int. J. Modern Phy. C* **2022**, *33*, 2250013.
35. Sunitha, M.; Gamaoun, F.; Abdulrahman, A.; Malagi, N.S.; Singh, S.; Gowda, R.J.; Gowda, R.J.P. An efficient analytical approach with novel integral transform to study the two-dimensional solute transport problem. *Ain Shams Eng. J.* **2022**, *14*, 101878. [[CrossRef](#)]
36. Gowda, R.J.P.; Naveenkumar, R.; Madhukesh, J.K.; Prasannakumara, B.C.; Gorla, R.S.R. Theoretical analysis of SWCNT-MWCNT/H<sub>2</sub>O hybrid flow over an upward/downward moving rotating disk. *Proc. Inst. Mech. Eng. Part N J. Nanomater. Nanoeng. Nanosyst.* **2021**, *235*, 97–106. [[CrossRef](#)]
37. Naveen Kumar, R.; Hogarehally, B.M.; Nirmala, T.; Punith Gowda, R.J.; Deepak, U.S. Carbon nanotubes suspended dusty nanofluid flow over stretching porous rotating disk with non-uniform heat source/sink. *Int. J. Comput. Methods Eng. Sci. Mech.* **2022**, *23*, 119–128. [[CrossRef](#)]
38. Naveen Kumar, R.; Gowda, R.J.P.; Giresha, B.J. Non-Newtonian hybrid nanofluid flow over vertically upward/downward moving rotating disk in a Darcy–Forchheimer porous medium. *Eur. Phys. J. Spec. Top.* **2021**, *230*, 1227–1237. [[CrossRef](#)]
39. Anwar Bég, O.; Mahabaleshwar, U.S.; Rashidi, M.M.; Rahimzadeh, N.; Curiel Sosa, J.L.; Sarris, I.; Laraqi, N. Homotopy analysis of magnetohydrodynamic convection flow in manufacture of a viscoelastic fabric for space applications. *Int. J. Appl. Math. Mech.* **2014**, *10*, 9–49.
40. Sowmya, G.; Varun Kumar, R.S.; Alsulami, M.D.; Prasannakumara, B.C. Thermal stress and temperature distribution of an annular fin with variable temperature-dependent thermal properties and magnetic field using DTM-Pade approximant. *Waves Random Complex Media* **2022**. [[CrossRef](#)]
41. Jayaprakash, M.C.; Alsulami, M.D.; Shanker, B.; Varun Kumar, R.S. Investigation of Arrhenius activation energy and convective heat transfer efficiency in radiative hybrid nanofluid flow. *Waves Random Complex Media* **2022**. [[CrossRef](#)]
42. Benos, L.T.; Polychronopoulos, N.D.; Mahabaleshwar, U.S. Thermal and flow investigation of MHD natural convection in a nanofluid-saturated porous enclosure: An asymptotic analysis. *J. Therm. Anal. Calorim.* **2021**, *143*, 751–765. [[CrossRef](#)]
43. Sowmya, G.; Sarris, I.E.; Vishalakshi, C.S.; Kumar, R.S.V.; Prasannakumara, B.C. Analysis of Transient Thermal Distribution in a Convective–Radiative Moving Rod Using Two-Dimensional Differential Transform Method with Multivariate Pade Approximant. *Symmetry* **2021**, *13*, 1793. [[CrossRef](#)]
44. Sahoo, B.; Poncet, S.; Labropulu, F. Effects of slip on the Von Kármán swirling flow and heat transfer in a porous medium. *Trans. Can. Soc. Mech. Eng.* **2015**, *39*, 357–366. [[CrossRef](#)]
45. Liao, S.J. Series Solution of Non-Similarity Boundary-Layer Flow in Porous Medium. The Proposed Homotopy Analysis Technique for the Solution of Non-Linear Problems. Ph.D. Thesis, Shanghai Jiao Tong University, Shanghai, China, 1992.
46. Liao, S.J. On the homotopy analysis method for nonlinear problems. *Appl. Math. Comp.* **2004**, *147*, 499–513. [[CrossRef](#)]
47. Liao, S.J. Analytic Solution for Fluid Flow over an Exponentially Stretching Porous Sheet with Surface Heat Flux in Porous Medium by Means of Homotopy Analysis Method. *Appl. Math. Comp.* **2005**, *169*, 1186–1194. [[CrossRef](#)]
48. Liao, S.J. Homotopy analysis method: A new analytical technique for nonlinear problems. *Commun. Nonlinear. Sci. Numer. Simul.* **1997**, *2*, 95–100. [[CrossRef](#)]
49. Hayat, T.; Javed, T.; Sajid, M. Analytic solution for rotating flow and heat transfer analysis of a third-grade fluid. *Acta Mechanica.* **2007**, *191*, 219–229. [[CrossRef](#)]
50. Abbasbandy, S. Solving Nonlinear Stochastic Diffusion Models with Nonlinear Losses Using the Homotopy Analysis Method. *Nonlinear Dyn.* **2008**, *51*, 83–87. [[CrossRef](#)]
51. Zhu, S.P. An Exact and Explicit Solution for the Valuation of American Put Options. *Quant. Financ.* **2006**, *6*, 229–242. [[CrossRef](#)]
52. Effati, S.; SaberiNik, H.; Shirazian, M. Analytic-approximate solution for a class of nonlinear optimal control problems by Homotopy analysis method Asian-Euro. *J. Math.* **2013**, *6*, 1–22.
53. Ahlersten, K. *An Introduction to MATLAB*; Bookboon: Copenhagen, Denmark, 2015.

**Disclaimer/Publisher’s Note:** The statements, opinions and data contained in all publications are solely those of the individual author(s) and contributor(s) and not of MDPI and/or the editor(s). MDPI and/or the editor(s) disclaim responsibility for any injury to people or property resulting from any ideas, methods, instructions or products referred to in the content.